Study of a double epi-layers SiC junction barrier Schottky rectifiers embedded P layer in the drift region*

Song Qing-Wen(宋庆文)†, Zhang Yu-Ming(张玉明), Zhang Yi-Men(张义门),
Zhang Qian(张 倩), and Lü Hong-Liang(吕红亮)

School of Microelectronics, Key Laboratory of Wide Band-Gap Semiconductor Materials and Devices, Xidian University, Xi'an 710071, China

(Received 19 October 2009; revised manuscript received 3 March 2010)

This paper proposes a double epi-layers 4H–SiC junction barrier Schottky rectifier (JBSR) with embedded P layer (EPL) in the drift region. The structure is characterized by the P-type layer formed in the n-type drift layer by epitaxial overgrowth process. The electric field and potential distribution are changed due to the buried P-layer, resulting in a high breakdown voltage (BV) and low specific on-resistance ($R_{\rm on,sp}$). The influences of device parameters, such as the depth of the embedded P+ regions, the space between them and the doping concentration of the drift region, etc., on BV and $R_{\rm on,sp}$ are investigated by simulations, which provides a particularly useful guideline for the optimal design of the device. The results indicate that BV is increased by 48.5% and Baliga's figure of merit (BFOM) is increased by 67.9% compared to a conventional 4H–SiC JBSR.

Keywords: junction barrier Schottky rectifier, 4H–SiC, breakdown voltage, specific on-resistance

PACC: 7210, 7220, 7280

1. Introduction

The SiC Schottky rectifiers have been proved to have great potential in power applications for their low conduction loss and fast switching speed.[1,2] The SiC junction barrier Schottky rectifiers (JBSR) have attracted much attention due to its advantages such as the Schottky-like on-state and fast switching characteristics together with the off-state characteristics having a lower leakage current similar to that of the pin rectifier.[3] The key issue in SiC power devices is to obtain a trade-off between breakdown voltage (BV) and specific on-resistance ($R_{\rm on,sp}$). However, a high BV requires a relatively thick and lowly doped drift region, which in turn leads to a high $R_{\rm on,sp}$. To solve this problem, super-junction concept[4] was proposed for Si power devices with oppositely doped regions in the drift region. Virtually, it is impossible to employ these structures for SiC device because of the extremely low diffusion rate of the dopant impurities or difficulties in achieving charge compensation between heavily doped n- and p-type pillars.[5,6] Recently, the P-buried floating junction (FJ) was proposed,[7–9] which does not require the charge compensation and can be achieved by multiple epitaxial overgrowth process.

Based on the FJ concept, a 4H–SiC JBSR embedded P layer (EPL) in the drift region is proposed in this paper. In blocking state, the EPL, which introduces a new peak electric field between the two regions and changes the body field distribution, enhances BV and lowers $R_{\rm on,sp}$. The influence of device parameters on BV and $R_{\rm on,sp}$ are investigated in detail utilizing two-dimensional (2D) semiconductor device simulator ISE-DESSISE.[10]

2. Structure and mechanism

Figure 1 is a schematic cross section of a JBSR–EPL. The t_1, t_2 and t_3 are the thickness of the 4H–SiC epi-layer 1, the EPL and epi-layer 2, respectively. The w_1, w_2 are the width of the surface P^+ regions and the embedded P^+ regions. The s_1, s_2 are the space between the surface P^+ regions and the embedded P^+ regions. In this paper, $t_1 = 14$ μm, $t_2 = 15.5$ μm, $t_3 = 0.5$ μm, $w_1 = w_2 = 1$ μm, and $s_1 = s_2 = 2$ μm. The drift region consists of epi-layer 1 and epi-layer 2 as shown in Fig. 1, with their doping concentration $N_{\rm d1} = N_{\rm d2} = 7 \times 10^{15}$ cm^{-3}. An n-type 4H–SiC substrate is used and the doping concentration of it is 1×10^{19} cm^{-3}.

*Project supported by the 13115 Innovation Engineering of Shaanxi Province of China (Grant No. 2008ZDKG-30).
†Corresponding author. E-mail: soqwe@126.com
© 2010 Chinese Physical Society and IOP Publishing Ltd

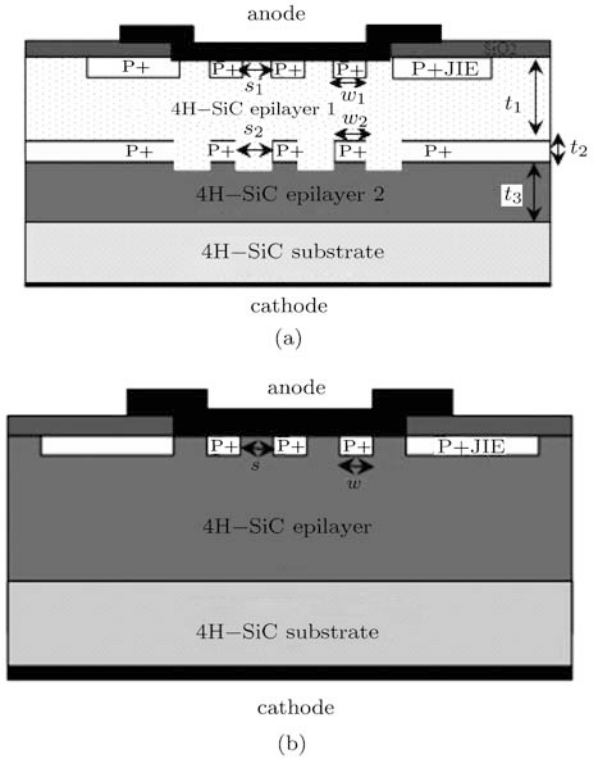


Fig. 1. (a) Schematic cross section of a 4H–SiC JBSR–EPL. (b) Schematic cross section of a conventional 4H–SiC JBSR.

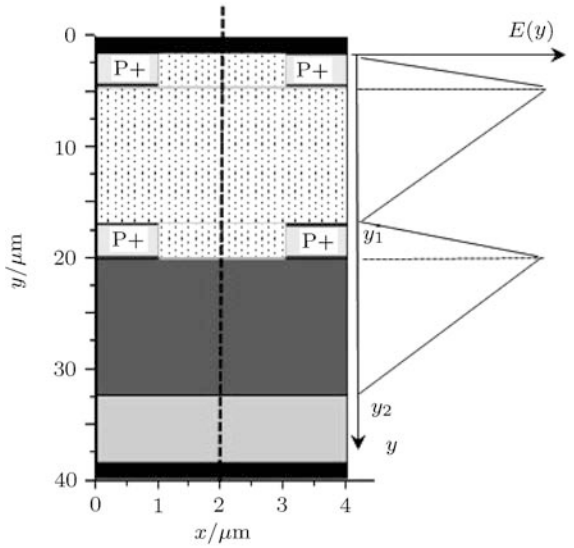


Fig. 2. Cell of a 4H–SiC JBSR–EPL.

When the device is in reverse bias, a depletion region is first formed in the epi-layer 1 together with the generation of a strong electric field to support the voltage. The one-dimensional (1D) Poisson's equation at $x = 2$ μm (as shown Fig. 2) for the epi-layer 1 is given by

$$\frac{\mathrm{d}^2V(y)}{\mathrm{d}y^2} = -\frac{\mathrm{d}E(y)}{\mathrm{d}y} = -\frac{qN_{\mathrm{d1}}}{\varepsilon_{\mathrm{s}}}, \tag{1}$$

where $V(y)$ is the applied voltage, $E(y)$ is the electric field, ε_{s} is the dielectric constant, and q is the electron charge. With the boundary condition that the electric field is zero at $y = y_1$ and the voltage is zero at $y = 0$, the electric field and the voltage distribution can be expressed as

$$E(y) = -\frac{qN_{\mathrm{d1}}}{\varepsilon_{\mathrm{s}}}(y_1 - y), \tag{2}$$

$$V(y) = -\frac{qN_{\mathrm{d1}}}{\varepsilon_{\mathrm{s}}}\left(y_1 \times x - \frac{x^2}{2}\right). \tag{3}$$

After the epi-layer 1 is depleted completely, the depletion region extends to the epi-layer 2 with increasing applied voltage. With the boundary that electric field is zero at $y = y_2$ and the voltage is V_1 at $y = y_1$, the electric field and voltage distribution are given by

$$E(y) = -\frac{qN_{\mathrm{d2}}}{\varepsilon_{\mathrm{s}}}(y_2 - y), \tag{4}$$

$$V(y) = -\frac{qN_{\mathrm{d2}}}{\varepsilon_{\mathrm{s}}}\left(y_1 y + y_1^2 - \frac{(y + y_1)^2}{2}\right) + V_1. \tag{5}$$

It is noted that in the blocking state, the EPL introduces a new electric field peak at the interface between the regions 1 and 2, which changes the electric field distribution in the drift region into two triangles. While, the electric field distribution of conventional JBSR is a single triangle. The blocking voltage corresponds to the sum area of triangle, which indicates that the $R_{\mathrm{on,sp}}$ of JBSR–EPL is half of that of conventional JBSR when the JBSR–EPL has the same BV as the conventional JBSR. So the BFOM of the device can be effectively increased compared to conventional JBSR. The BFOM is used to evaluate the device characteristics, which can be expressed as[11]

$$\mathrm{BFOM} = \varepsilon_{\mathrm{s}}\mu_{\mathrm{n}}E_{\mathrm{M}} = \frac{4V_{\mathrm{Breakdown}}^2}{R_{\mathrm{on,sp}}}, \tag{6}$$

where the ε_s is the dielectric constant, μ_{n} is the electron mobility, and E_{M} is the critical electric field.

3. Results and discussion

All simulations are performed at 300 K with the recently available material parameters for 4H–SiC.[12−14] The comparisons of the simulated I–V characteristics of the conventional 4H–SiC JBSR with the experimental data are shown in Fig. 3 and they match very well, which verifies that the presented models are suitable.

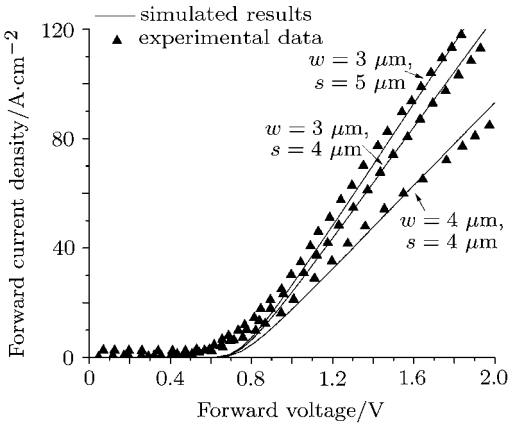


Fig. 3. Comparison of simulated forward I–V with experimental data from Ref. [15].

Figure 4 shows the two-dimensional (2D) electric field distribution of the 4H–SiC JBSR–EPL and conventional 4H–SiC JBSR (JBSR1). Figure 5 shows the electric field and potential distribution of them along y direction at $x = 2$ μm (in the middle of the drift region). By comparison, the electric field distributions are in agreement with the analysis results presented in Section 2. As shown in Fig. 5(a), the 4H–SiC JBSR–EPL has a new electric field peak at the interface of the epi-layers. Therefore, the EPL reduces the electric field in the epi-layer 1, avoiding premature breakdown at the surface and leading to a higher BV than that of the conventional 4H–SiC JBSR.

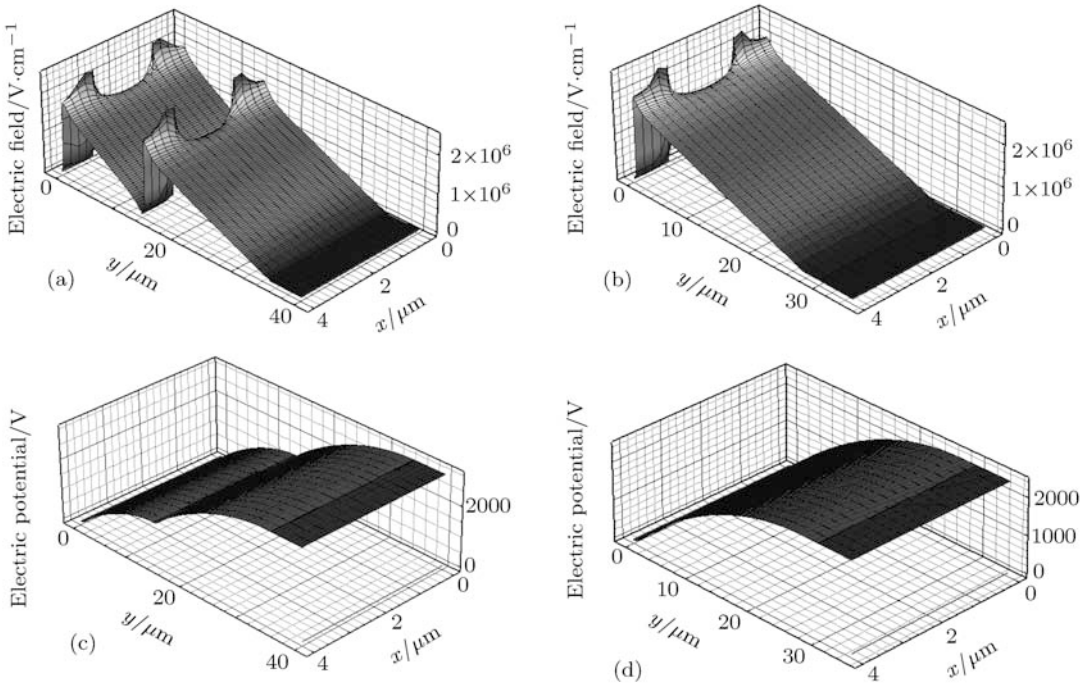


Fig. 4. (a) The 2D electric field distribution of the 4H–SiC JBSR–EPL ($N_{d1} = N_{d2} = 7 \times 10^{15}$ cm^{-3}) for a reverse bias of 2500 V. (b) The 2D electric field distribution of the 4H–SiC JBSR1 ($N_d = 3.5 \times 10^{15}$ cm^{-3}) for a reverse bias of 2500 V. (c) The 2D electric potential distribution of the 4H–SiC JBSR–EPL ($N_{d1} = N_{d2} = 7 \times 10^{15}$ cm^{-3}) for a reverse bias of 2500 V. (d) The 2D electric potential distribution of the 4H–SiC JBSR1 ($N_d = 3.5 \times 10^{15}$ cm^{-3}) for a reverse bias of 2500 V.

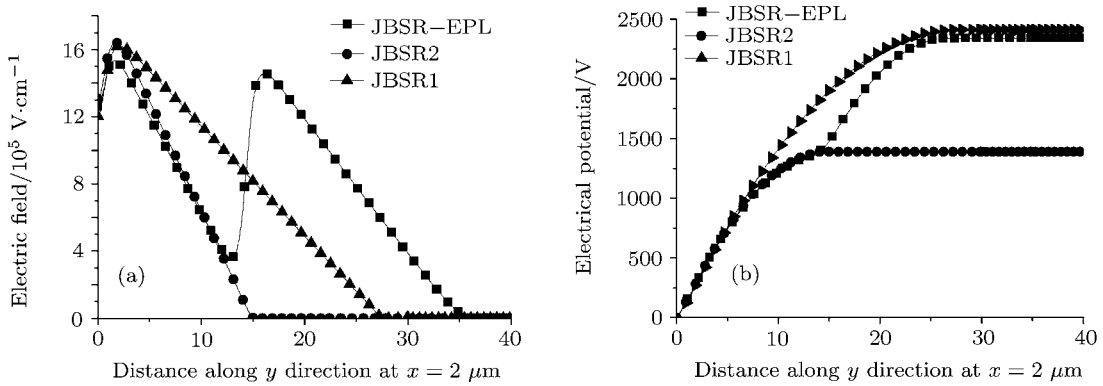


Fig. 5. (a) Electric field distribution of the 4H–SiC JBSR–EPL, JBSR1 ($N_d = 3.5 \times 10^{15}$ cm^{-3}) and JBSR2 ($N_d = 7 \times 10^{15}$ cm^{-3}) at $x = 2$ μm. (b) Potential distribution of the 4H–SiC JBSR–EPL, JBSR1 and JBSR2 at $x = 2$ μm.

The forward and reverse I–V characteristics of the 4H–SiC JBSR–EPL, JBSR1 and JBSR2 are shown in Fig. 6. When $N_{d1} = N_{d2} = 7 \times 10^{15}$ cm^{-3}, the BV of the 4H–SiC JBSR–EPL is 2432 V and $R_{on,sp}$ = 6.3 mΩ·cm^2. While, the same doping concentration applied to the conventional JBSR (JBSR2), the BV=1252 V and $R_{on,sp}$=5.2 mΩ·cm^2. The BV of the 4H–SiC JBSR–EPL is increased by 48.5% and $R_{on,sp}$ is only increased by 14.2% compared with the JBSR2. The BFOM of 4H–SiC JBSR–EPL is increased by 67.9% compared with the JBSR2. For the JBSR1 doped $N_d = 3.5 \times 10^{15}$ cm^{-3}, the BV=2486 V and $R_{on,sp}$=9.7 mΩ·cm^2. Even though the BV for the JBSR1 is 2.1% higher than that of JBSR–EPL, its $R_{on,sp}$ is increased by 36.1%. The BFOM of 4H–SiC JBSR–EPL is 32.1% higher than that of the JBSR1. It indicates that the trade-off between BV and $R_{on,sp}$ is significantly improved.

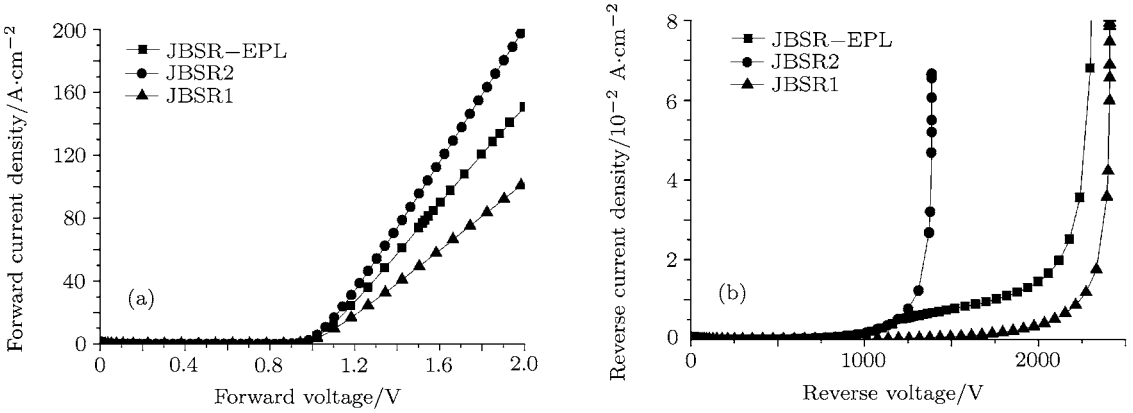


Fig. 6. (a) Forward I–V characteristics of the 4H–SiC JBSR–EPL ($N_{d1} = N_{d2} = 7 \times 10^{15}$ cm^{-3}), JBSR1 ($N_d = 3.5 \times 10^{15}$ cm^{-3}) and JBSR2 ($N_d = 7 \times 10^{15}$ cm^{-3}). (b) Reverse I–V characteristics of the 4H–SiC JBSR–EPL, JBSR1 and JBSR2.

Figure 7 illustrates the dependences of BV of the 4H–SiC JBSR–EPL on t_1 and t_2, while keeping the sum of t_1 and t_2 equals 34.5 μm. It demonstrates that a maximum BV is achieved at $t_1 = 10$ μm, 14 μm and 17 μm for three different drift concentrations of N_{d1}=9×10^{15} cm^{-3} > $N_{d2} = 7 \times 10^{15}$ cm^{-3}, $N_{d1} = N_{d2} = 7 \times 10^{15}$ cm^{-3}, and N_{d1}=5×10^{15} cm^{-3} < $N_{d2} = 7 \times 10^{15}$ cm^{-3} respectively, and t_1 must be precisely controlled during design and process. The comparison of the electric field distribution of the 4H–SiC JBSR–EPL ($N_{d1} = N_{d2} = 7 \times 10^{15}$ cm^{-3}) at $x = 2$ μm for different t_1 at breakdown point is presented in Fig. 8. At t_{1opt} of the optimum value of t_1, the first electric field peak equals the second electric field peak. When t_1 is less than t_{1opt}, the first electric field peak increases with the increased t_1, while the

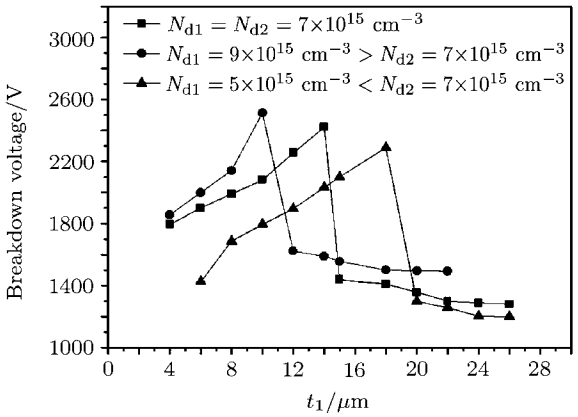


Fig. 7. Breakdown voltage of 4H–SiC JBSR–EPL versus the depth of EPL t_1.

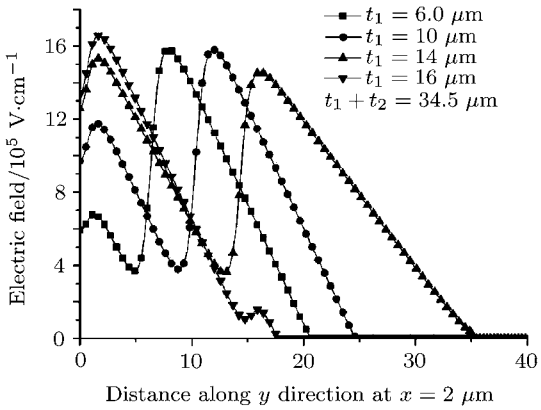


Fig. 8. Electric field distribution of JBSR–EPL ($N_{d1} = N_{d2} = 7 \times 10^{15}$ cm^{-3}) along y direction at $x = 2$ μm for different t_1 at breakdown point.

second electric filed peak slightly changes. When t_1 is larger than $t_{1\mathrm{opt}}$, the second electric field peak reduces rapidly.

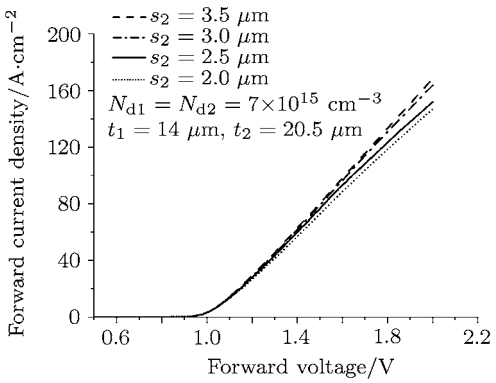


Fig. 9. Forward characteristics of the 4H–SiC JBSR–EPL with different w_2 and s_2.

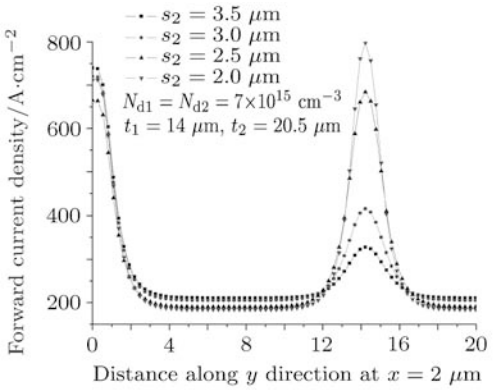


Fig. 10. Vertical current density contribution of the 4H–SiC JBSR–EPL at $x = 2\ \mu$m with different w_2 and s_2 at 2 V.

Figure 9 shows the simulated forward characteristics of the 4H–SiC JBSR–EPL with different w_2 and s_2, while keeping the sum of the $2 \times w_2$ and s_2 to be equal to 4 μm. It can be seen that $R_{\mathrm{on,sp}}$ increases with the increased s_2. Figure 10 gives the vertical current density contribution of the 4H–SiC JBSR–EPL at $x = 2\ \mu$m with different w_2 and s_2 at 2 V. This can be explained by the depletion layer extension from the embedded p–n junction, which blocks the current flow, leading to the accumulation of electrons and change of the $R_{\mathrm{on,sp}}$. Reverse I–V of the 4H–SiC JBSR–EPL with different w_2 and s_2 are shown in Fig. 11, which indicates that the BV decreases with the increased s_2. So there is a trade-off between the $R_{\mathrm{on,sp}}$ and BV in the optimal design of w_2 and s_2.

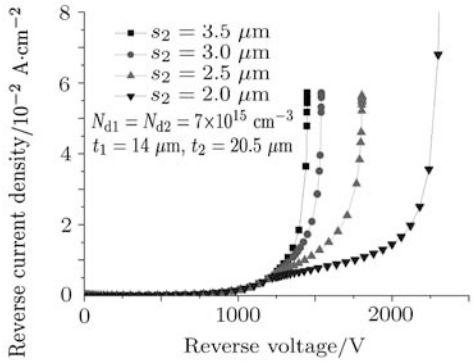


Fig. 11. Reverse I–V of the 4H–SiC JBSR–EPL with different w_2 and s_2.

4. Conclusions

In this paper, a double epi-layers 4H–SiC JBSR with EPL in the drift region is proposed. The mechanism of the device has been discussed by the solution from solving the 1D Poisson's equation and elaborate simulation results from 2D simulator, which indicate that the trade-off between BV and $R_{\mathrm{on,sp}}$ and BFOM can be significantly improved compared to a conventional 4H–SiC JBSR. The influence of device parameters such as the depth of the EPL t_1, t_2, the space between embedded P regions and the doping concentration of the drift region on BV and $R_{\mathrm{on,sp}}$ are also investigated in detail. The electric field distribution can be significantly changed with different t_1, which should be precisely controlled during design and process. To achieve high BV and low $R_{\mathrm{on,sp}}$ of the device, the trade-off between s_2 and BV should be considered in the optimal design of the 4H–SiC JBSR with EPL.

References

[1] Toru H, Tsutomu H, Jun S and Tsunenobu K 2008 *IEEE Trans. Electron Devices* **55** 1841

[2] Cao Q J, Zhang Y M and Zhang Y M 2008 *Chin. Phys.* B **17** 4622

[3] Sang-Cheol Kim, Wook Bahng, In-Ho Kang, Sung-Jae Joo and Nam-Kyun Kim 2008 *Proc. 26th Int. Conf. on Microelectronics* pp. 181–184

[4] Fujihira T 1997 *Jpn. J. Appl. Phys.* **36** 6254

[5] Nishio Johji, Ota Chiharu, Hatakeyama Tetsuo, Shinohe Takashi, Kojima Kazutoshi, Nishizawa Shin-Ichi and Ohashi Hiromichi 2008 *IEEE Trans. Electron Devices* **45** 1954

[6] Liang C Y and Kuang S 2008 *IEEE Trans. Electron Devices* **55** 1961

[7] Cézac N, Moranch F, Rossel P, Tranduc H and Peyre-Lavigne A 2000 *Proc. 12th Int. Symp. Power Semicond. Devices ICs* Toulouse France pp. 69–72
[8] Saitoh W, Omura I, Tokano K, Ogura T and Ohashi H 2002 *14th Int. Sym. Power Semicond. Devices ICs* pp. 33–36
[9] Chen X B, Wang X and Sin J K O 2000 *IEEE Trans. Electron Devices* **47** 1280
[10] DESSIS-ISE, *2D Semiconductor Device Simulator* version 10.0 2005 Integrated Systems Engineerin, Zurich
[11] Baliga B J 1989 *IEEE Electron Device Lett.* **10** 455
[12] Chante J P, Locatelli M L, Planson D, Ottaviani L, Morvan E, Isoird K and Nallet F 1998 *Proc CAS Int. Semicond. Conf.* pp. 125–134
[13] Roschke M and Schwierz F 2001 *IEEE Trans. Electron Devices* **48** 1442
[14] Jarrendahl K and Davis R F 1998 *Semiconductors and Semimetals* **52** 1
[15] Zhu L, Chow T P, Jones K A and Agarwal A 2006 *IEEE Trans. Electron Devices* **53** 363